Available online at www.sciencedirect.com
ScienceDirect
Journal of Power Sources 158 (2006) 1414–1418
JOURNAL OF POWER SOURCES
www.elsevier.com/locate/jpowsour

Short communication

Electrochemical properties of $LiCr_xNi_{0.5-x}Mn_{0.5}O_2$ prepared by co-precipitation method for lithium secondary batteries

Guk-Tae Kim [a], Jong-Uk Kim [b], Young-Jae Sim [c], Ki-Won Kim [d,*]

[a] *Advanced Material Research Center, Engineering Research Institute, Gyeongsang National University, 900 Gajwa-dong, Jinju 660-701, South Korea*
[b] *Korea Association of Aids to Navigation, Wonjeong-ri Poseung-myeon, Pyeongtaek 451-822, South Korea*
[c] *Department of Ceramic Engineering, Gyeongsang National University, 900 Gajwa-dong, Jinju 660-701, South Korea*
[d] *Department of Metallurgical and Materials Engineering and ITRC for Energy Storage and Conversion, Gyeongsang National University, 900 Gajwa-dong, Jinju 660-701, South Korea*

Received 14 June 2005; accepted 12 October 2005
Available online 7 December 2005

Abstract

The purpose of this research is to study a new synthesis of $LiCr_xNi_{0.5-x}Mn_{0.5}O_2$ ($x = 0$, 0.05 and 0.1) using a co-precipitation method for lithium secondary batteries. Investigations are made of the morphology, cyclic voltammetry and charge–discharge cycling of $LiCr_xNi_{0.5-x}Mn_{0.5}O_2$/Li cells. The particle size of $LiNi_{0.5}Mn_{0.5}O_2$ has a narrow distribution range from 200 to 300 nm. The peak current of $LiCr_{0.05}Ni_{0.45}Mn_{0.5}O_2$ and $LiCr_{0.1}Ni_{0.4}Mn_{0.5}O_2$ in the 2.7 and 2.9 V regions increases with increasing addition of Cr in $LiCr_xNi_{0.5-x}Mn_{0.5}O_2$. The discharge capacity of the $LiNi_{0.5}Mn_{0.5}O_2$ electrode is 185 and 150 mAh g^{-1} at 1 and 15 cycles, respectively. The fading in capacity of Cr-doped $LiNi_{0.5}Mn_{0.5}O_2$ is less than that of $LiNi_{0.5}Mn_{0.5}O_2$ during cycling. $LiCr_xNi_{0.5-x}Mn_{0.5}O_2$ cathodes with 1 M $LiPF_6$ in an ethyl carbonate–dimethyl carbonate (EC–DMC) electrolyte exhibit good cycling performance.

Keywords: $LiCr_xNi_{0.5-x}Mn_{0.5}O_2$; Nanoparticle; Co-precipitation; Lithium secondary battery; Cycling performance; Discharge capacity

1. Introduction

The Li-ion battery is a suitable power source for a wide range of applications, such as microelectronics, electric vehicle batteries and load-levelling batteries. Using $LiCoO_2$ as a cathode material in commercial Li-ion batteries incurs the disadvantages of high cost, toxicity and insufficient capacity. There have been many attempts replace $LiCoO_2$, namely through the use of $LiNiO_2$ [1,2], $LiMnO_2$ [3,4] or Co–Ni [5,6] and Mn–Co–Ni [7,8] mixed oxides. $LiNiO_2$ and $LiMnO_2$ are attractive cathode materials because of their relatively low cost and high capacity. On the other hand, these two oxides are difficult to synthesize, have poor cycle at high voltage (4.3 V versus Li^+/Li) [9], and suffer Jahn-teller distortion of the MnO_6 octahedra that leads to eventual degradation of electrode performance [8]. Ohzuku et al. [10] reported $LiNi_{1/3}CO_{1/3}Mn_{1/3}O_2$ with excellent cycling properties and high discharge capacity (about 160 mAh g^{-1}), but this material includes Co that is expensive and toxic.

Recently, $LiNi_{0.5}Mn_{0.5}O_2$ similar to a solid-state mixture of $LiNiO_2$ and $LiMnO_2$ was reported by Ohzuku et al. [10]. The material has a hexagonal O_3 structure similar to that of α-$NaFeO_2$ ($R\bar{3}m$) and also a suitable conduction pathway that is composed of an alternating-layer arrangement for Li^+ ions during the charge–discharge process [11]. Spahr et al. [12] demonstrated that this material could be synthesized as single-phase $LiMn_xNi_{1-x}O_2$ by using a co-precipitation method; the initial capacity was about 170 mAh g^{-1}.

In the co-precipitation method, most of the pure-phase $LiNi_{0.5}Mn_{0.5}O_2$ is synthesized by using the hydroxide method. In general, cathode materials synthesized by the co-precipitation method have uniform particles and high capacity. The application of Cr-doped lithium manganese materials, such as $LiCr_xMn_{2-x}O_4$ and $LiCr_xMn_{1-x}O_2$ cathodes has been examined in liquid electrolytes [13,14].

In this study, nanosized $LiCr_xNi_{0.5-x}Mn_{0.5}O_2$ has been prepared by a co-precipitation method with K_2CO_3 as the precip-

* Corresponding author. Tel.: +82 55 751 5305; fax: +82 55 751 6539.
E-mail address: kiwonkim@gsnu.ac.kr (K.-W. Kim).

0378-7753/$ – see front matter © 2005 Published by Elsevier B.V.
doi:10.1016/j.jpowsour.2005.10.074

itation agent and has been applied as a cathode material for Li secondary batteries.

2. Experimental

$LiNi_{0.5}Mn_{0.5}O_2$, $LiCr_{0.05}Ni_{0.45}MnO_2$ and $LiCr_{0.1}Ni_{0.4}Mn_{0.5}O_2$ were synthesized by the co-precipitation method. The precipitation agent was K_2CO_3 (Aldrich). A stoichiometric amount of $Mn(SO_4)\cdot H_2O$ (>98%, Aldrich) and $Ni(SO_4)\cdot 6H_2O$ (>98%, Aldrich) was dissolved in distilled water, and the required amount of K_2CO_3 was also dissolved in distilled solution. Into the solution of the precipitation agent (2 mol L^{-1}), a solution of Mn and Ni sulfates (2 M) was added and stirred for about 1 h. The metal oxalate precipitates were washed with distilled water for several times to remove SO_4^{2-} and K^+. A 2 M solution of $LiOH\cdot H_2O$ (>98%, Aldrich) or $LiOH\cdot H_2O$ and $CrCl_3\cdot 6H_2O$ (>98%, Aldrich) in the stoichiometric ratio was added into a continuously agitated solution of the precipitate. The resultant solution was dried with a rotary evaporator at 40 °C to obtain the precursor that was preheated at 550 °C for 5 h and then calcined at 900 °C for 12 h. The thermal decomposition behaviour of each precursor was examined by themorgravimetric analysis (TGA) and differential thermal analysis (DTA) (TG–DTA, G-DTA16 and SETARAM). The structure of the sample was characterized by X-ray diffraction (D5005, Siemens) with Cu Kα radiation. The particle morphology was observed using a field emission scanning electron microscope (FE-SEM XL30SLF, Philips).

A composite cathode slurry was prepared by mixing a given $LiCr_xNi_{0.5-x}Mn_{0.5}O_2$ ($x=0$, 0.05 and 0.1) powder with carbon black (super-P, MMM Carbon) and polyvinylidenefluoride (PVDF, Aldrich) in *N*-methylpyrrolidinone (NMP, Aldrich) solution. The electrode composite was 70:15:15 wt.% mixture of active material, electrical conductor and binder, respectively. The slurry mixture was ball-milled using a planetary miller at 250 rpm for 30 min. The composite film was prepared by coating this slurry on to an Al foil current-collector.

After evaporating the solvent, the composite film was vacuum-dried at 100 °C for 24 h. The electrochemical behaviour of the composite film was investigated in three-electrode cells with 1 M $LiPF_6$ in ethyl carbonate–dimethyl carbonate (EC–DMC) (Cheil industries). The composite films were used as working electrodes. Pure lithium metal was used for both the counter and the reference electrodes. Cyclic voltammetry was carried out between 2.5 and 4.6 V versus Li/Li^+ at a scan rate of 0.1 mV s^{-1}. The components of each charge–discharge test cell were stacked in a 2032 coin-type cell (Hohsen) with a single Li foil as the counter and the reference electrodes. The size of each cell was 1 cm^2. The current for charge–discharge cycling was the 0.1*C* rate between 2.6 and 4.5 V versus Li/Li^+ using a battery cycler. All the preparation and testing of the cells were conducted in an argon-filled glove box.

3. Results and discussion

The TGA and DTA results for the precursors of $LiNi_{0.5}Mn_{0.5}O_2$, are shown in Fig. 1. The first weight loss before 180 °C is due to the loss of absorbed water in the mixed precursors of $NiCO_3\cdot xH_2O$ and $MnCO_3\cdot xH_2O$. There is a further weight loss between 180 and 400 °C that is attributable to the decomposition of nickel carbonate [15]. Finally, weight loss between 400 and 700 °C is due to the decomposition of $MnCO_3$ [16]. The TGA and DTA curves for the precursors of $LiCr_{0.05}Ni_{0.45}MnO_2$ and $LiCr_{0.1}Ni_{0.4}Mn_{0.5}O_2$ yield similar results.

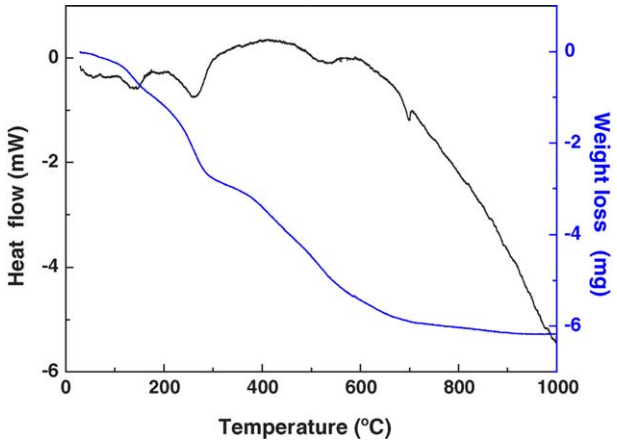

Fig. 1. TG–DTA curves for $LiNi_{0.5}Mn_{0.5}O_2$ precursor prepared by co-precipitation method.

The XRD patterns for $LiCr_xNi_{0.5-x}Mn_{0.5}O_2$ ($x=0$, 0.05 and 0.1) powders prepared by co-precipitation are presented in Fig. 2. According to the JCPDS reference, the $LiCr_xNi_{0.5-x}Mn_{0.5}O_2$ peaks at (0 0 3), (1 0 1) and (1 0 4) correspond to the typical α-$NaFeO_2$ ($R\bar{3}m$) layered structure [10]. The intensity ratio of the (1 0 4) peak to the (0 0 3) peak is about 0.5. Impurity phases are not present in $LiNi_{0.5}Mn_{0.5}O_2$, $LiCr_{0.05}Ni_{0.45}Mn_{0.5}O_2$ and $LiCr_{0.1}Ni_{0.4}Mn_{0.5}O_2$ powders.

The morphology of $LiNi_{0.5}Mn_{0.5}O_2$, $LiCr_{0.05}Ni_{0.45}MnO_2$ and $LiCr_{0.1}Ni_{0.4}Mn_{0.5}O_2$ powders is shown in Fig. 3. The $LiCr_xNi_{0.5-x}Mn_{0.5}O_2$ powder has a uniform distribution with

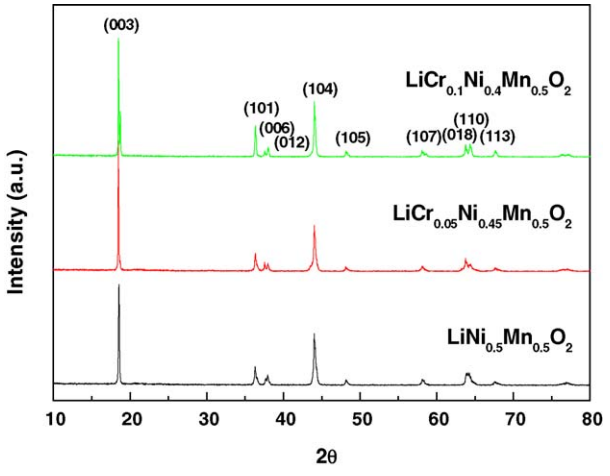

Fig. 2. XRD patterns of $LiCr_xNi_{0.5-x}Mn_{0.5}O_2$ powders calcined at 900 °C for 12 h in air.

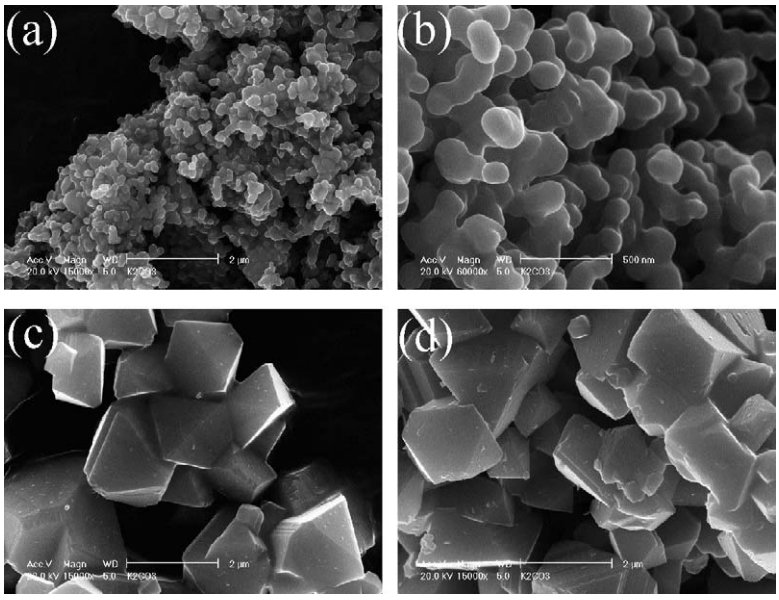

Fig. 3. Scanning electron micrographs of $LiCr_xNi_{0.5-x}Mn_{0.5}O_2$ powders calcined at 900 °C for 12 h in air: (a) $LiNi_{0.5}Mn_{0.5}O_2$, (b) $LiNi_{0.5}Mn_{0.5}O_2$, (c) $LiCr_{0.05}Ni_{0.45}Mn_{0.5}O_2$ and (d) $LiCr_{0.1}Ni_{0.4}Mn_{0.5}O_2$.

fine particles. The particle size of $LiNi_{0.5}Mn_{0.5}O_2$ covers a narrow distribution range from 200 to 300 nm. The growth and shape change of the powders occurs as the content of Cr in $LiCr_xNi_{1-x}Mn_{0.5}O_2$ ($x = 0$, 0.05 and 0.1) increases. The spherical shape of the $LiNi_{0.5}Mn_{0.5}O_2$ powder becomes octahedral with increasing Cr content. This change in shape is due to the variation in surface energy. The particle size of $LiCr_xNi_{1-x}Mn_{0.5}O_2$ ($x = 05$ and 0.1) is lager than that of $LiNi_{0.5}Mn_{0.5}O_2$ because the surface energy of its crystals is higher [17,18].

The cyclic voltammogram for $LiCr_xNi_{0.5-x}Mn_{0.5}O_2$/Li cells on the first cycle is given in Fig. 4. The cyclic voltammogram for the $LiNi_{0.5}Mn_{0.5}O_2$/Li cell has an oxidation peak in the 3.9 V region and a reduction peak in the 3.7 V region. The absence of a peak around 3 V suggests that manganese does not remain in the Mn^{3+} state. These peaks can be assigned to a Ni^{2+}/Ni^{4+} electrochemical process [13,19,20]. The development of the peaks appears to be slow. These observations on $LiNi_{0.5}Mn_{0.5}O_2$/Li cell are similar to these reported by Wu et al. [21]. On the other hand, the cyclic voltammograms of $LiCr_{0.05}Ni_{0.45}Mn_{0.5}O_2$ and $LiCr_{0.1}Ni_{0.4}Mn_{0.5}O_2$ have oxidation peaks in the 2.9, 3.9 and 4.4 V regions and reduction peaks in the 2.7 and 3.6 V regions. The peaks below 3 V correspond to the redox couple Cr^{3+}/Cr^{4+} [14,22]. The peak currents in the 2.7 and 2.9 V regions increase with increasing addition of Cr in $LiCr_xNi_{0.5-x}Mn_{0.5}O_2$.

The initial discharge curves of $LiCr_xNi_{0.5-x}Mn_{0.5}O_2$ cathodes in 1 M $LiPF_6$/EC–DMC at room temperature are presented in Fig. 5. Cycling was carried out between 4.5 and

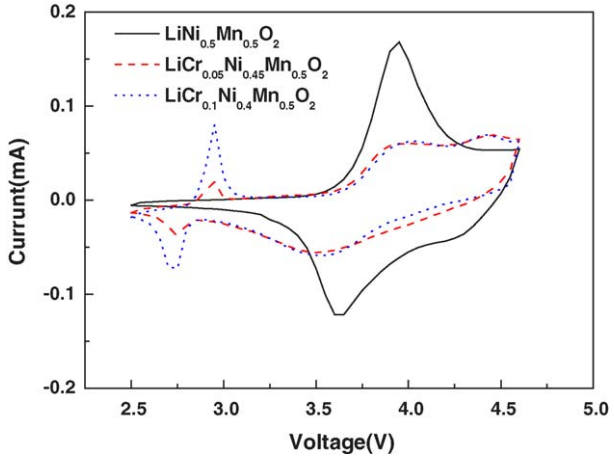

Fig. 4. Cyclic voltammograms for $LiCr_xNi_{0.5-x}Mn_{0.5}O_2$/Li cells as a function of addition ratio of Cr at a scan rate of 0.1 mV s^{-1}.

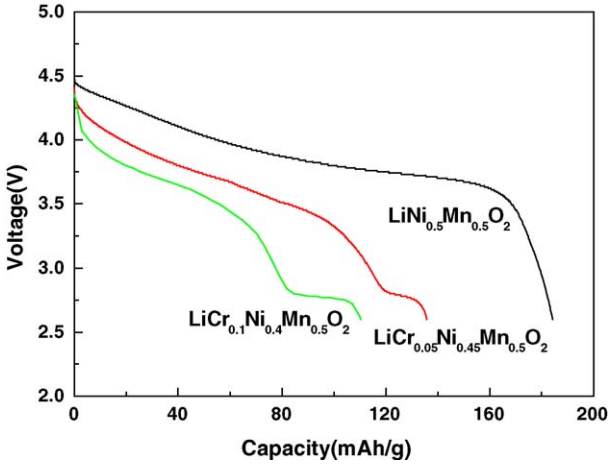

Fig. 5. Initial curves for $LiCr_xNi_{0.5-x}Mn_{0.5}O_2$/Li cells with 1 M $LiPF_6$/EC–DMC at 0.1*C* rate.

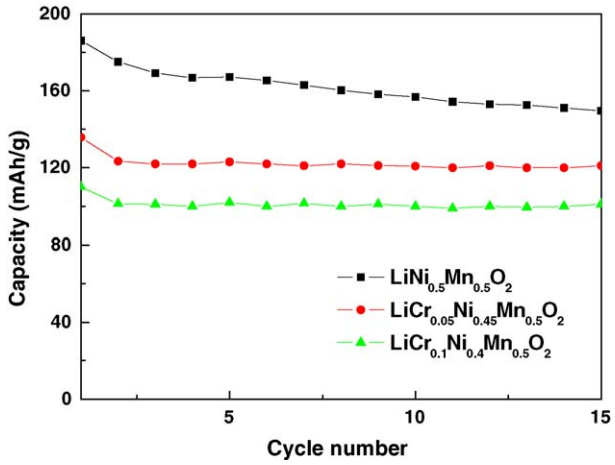

Fig. 6. Discharge capacity of $LiCr_xNi_{0.5-x}Mn_{0.5}O_2$/Li cells as a function of addition ratio of Cr on cycling at room temperature.

2.6 V at a current rate of 0.1*C*. The initial open-circuit voltage of $LiCr_xNi_{0.5-x}Mn_{0.5}O_2$/Li cells is 3.1 V. On the first discharge of the $LiNi_{0.5}Mn_{0.5}O_2$/Li cell, a voltage plateau appears around 3.8 V. The profile of discharge curve appears to be typical in $LiNi_{0.5}Mn_{0.5}O_2$. The first discharge capacity of the $LiNi_{0.5}Mn_{0.5}O_2$ electrode is 185 mAh g^{-1}, based on active material, and the utilization of $LiNi_{0.5}Mn_{0.5}O_2$ is 66%. The discharge curves of $LiCr_{0.05}Ni_{0.45}Mn_{0.5}O_2$ and $LiCr_{0.1}Ni_{0.4}Mn_{0.5}O_2$ cathodes display two voltage plateaus. The voltage plateau around 2.7 V increases with increasing addition of Cr in $LiCr_xNi_{0.5-x}Mn_{0.5}O_2$ and this corresponds to the cyclic voltammetric results obtained for $LiCr_xNi_{0.5-x}Mn_{0.5}O_2$/Li cells. The first discharge capacity of the $LiCr_{0.05}Ni_{0.45}Mn_{0.5}O_2$ and $LiCr_{0.1}Ni_{0.4}Mn_{0.5}O_2$ electrodes is 135 and 110 mAh g^{-1}, respectively. These data imply that the capacity of $LiCr_xNi_{0.5-x}Mn_{0.5}O_2$ decreases with increasing of addition of Cr due to the redox couple Cr^{3+}/Cr^{4+}.

The discharge capacity of $LiCr_xNi_{0.5-x}Mn_{0.5}O_2$/Li cells in 1 M $LiPF_6$ in EC–DMC is a given in Fig. 6 as a function of the addition ratio of Cr during charge–discharge cycling at room temperature. Cycling was conducted between 4.5 and 2.6 V at a current rate of 0.1*C*. The discharge capacity of the $LiNi_{0.5}Mn_{0.5}O_2$ electrode is 185 and 150 mAh g^{-1} on cycles 1 and 15 at room temperature, respectively. Thus, $LiNi_{0.5}Mn_{0.5}O_2$ provides a high capacity cathode material for Li secondary batteries. After the 5th cycle, the discharge capacity of $LiNi_{0.5}Mn_{0.5}O_2$ decreases slowly. The discharge capacities of $LiCr_{0.05}Ni_{0.45}Mn_{0.5}O_2$ and $LiCr_{0.1}Ni_{0.4}Mn_{0.5}O_2$ are smaller than that of $LiNi_{0.5}Mn_{0.5}O_2$ as a function of addition ratio of Cr. The capacity of $LiCr_{0.05}Ni_{0.45}Mn_{0.5}O_2$ is higher than that of $LiCr_{0.1}Ni_{0.4}Mn_{0.5}O_2$ until the 15th cycle. The fading in capacity of Cr-doped $LiNi_{0.5}Mn_{0.5}O_2$ is less than that of $LiNi_{0.5}Mn_{0.5}O_2$ during cycling; the charge–discharge efficiency is above 98% after the 2nd cycle. Further work is in progress to optimize the performance of $LiCr_xNi_{0.5-x}Mn_{0.5}O_2$ cathodes in liquid electrolyte. From these findings, it is conducted that $LiCr_xNi_{0.5-x}Mn_{0.5}O_2$ prepared by a co-precipitation method in 1 M $LiPF_6$ + EC–DMC electrolyte exhibits good capacity and stability with cycling.

4. Conclusions

$LiCr_xNi_{0.5-x}Mn_{0.5}O_2$ powder has a uniform distribution with fine particles. The particle size of $LiNi_{0.5}Mn_{0.5}O_2$ show a narrow distribution of range from 200 to 300 nm. Cyclic voltammograms of $LiCr_{0.05}Ni_{0.45}Mn_{0.5}O_2$ and $LiCr_{0.1}Ni_{0.4}Mn_{0.5}O_2$ reveal oxidation peaks in the 2.9, 3.9 and 4.4 V regions and reduction peaks in the 2.7 and 3.6 V regions. The peak current of $LiCr_{0.05}Ni_{0.45}Mn_{0.5}O_2$ and $LiCr_{0.1}Ni_{0.4}Mn_{0.5}O_2$ in the 2.7 and 2.9 V regions increases with increasing addition ratio of Cr in $LiCr_xNi_{0.5-x}Mn_{0.5}O_2$. On the first discharge of a $LiNi_{0.5}Mn_{0.5}O_2$/Li cell, a voltage plateau appears at around 3.8 V. By contrast, $LiCr_{0.05}Ni_{0.45}Mn_{0.5}O_2$ and $LiCr_{0.1}Ni_{0.4}Mn_{0.5}O_2$ cathodes give two voltage plateaus. The discharge capacity of the $LiNi_{0.5}Mn_{0.5}O_2$ electrode is 185 and 150 mAh g^{-1} at cycles 1 and 15, respectively. The discharge capacities of $LiCr_{0.05}Ni_{0.45}Mn_{0.5}O_2$ and $LiCr_{0.1}Ni_{0.4}Mn_{0.5}O_2$ were smaller than that of $LiNi_{0.5}Mn_{0.5}O_2$ as a function of Cr addition. The fading in capacity of Cr-doped $LiNi_{0.5}Mn_{0.5}O_2$ is less than that of $LiNi_{0.5}Mn_{0.5}O_2$ during charge–discharge cycling. It is conducted that $LiCr_xNi_{0.5-x}Mn_{0.5}O_2$ can be used for high-capacity materials, such as cathode materials for Li secondary batteries.

Acknowledgement

This work was supported by a Korea Research Foundation Grant (KRF-2004-005-B00252) and University IT Research Center Project.

References

[1] M.Y. Song, R. Lee, J. Power Sources 111 (2002) 97–103.
[2] B.V.R. Chowdari, G.V. Subba Rao, S.Y. Chow, Solid State Ionics 140 (2001) 55–62.
[3] C.-H. Lu, H.-C. Wang, J. Eur. Ceram. Soc. 24 (2004) 717–723.
[4] J.-U. Kim, Y.-J. Jo, G.-C. Park, W.-J. Jeong, H.-B. Gu, J. Power Sources 119–121 (2003) 686–689.
[5] J. Cho, Chem. Mater. 12 (2000) 3089–3094.
[6] Y. Kida, K. Yanagida, A. Yanai, A. Funahashi, T. Nohma, I. Yonezu, J. Power Sources 142 (2005) 323–328.
[7] Y.M. Todorov, K. Numata, Electrochim. Acta 50 (2004) 495–499.
[8] S.W. Oh, S.H. Park, C.-W. Park, Y.-K. Sun, Solid State Ionics 171 (2004) 167–172.
[9] L. Zhang, H. Noguchi, M. Yoshio, J. Power Sources 110 (2002) 57–64.
[10] T. Ohzuku, Y. Makimura, Chem. Lett. (2001) 642–643.
[11] S.H. Choi, O.A. Shlyakhtin, J. Kim, Y.S. Yoon, J. Power Sources 140 (2005) 355–360.
[12] M.E. Spahr, P. Novák, O. Haas, R. Nesper, J. Power Sources 68 (1997) 629–633.
[13] Z.P. Guo, G.X. Wang, H.K. Liu, S.X. Dou, Solid State Ionics 148 (2002) 359–366.
[14] X. Wu, S.H. Chang, Y.H. Park, K.S. Ryu, J. Power Sources 137 (2004) 105–110.
[15] L. Xiang, X.Y. Deng, Y. Jin, Scripta Mater. 47 (2002) 219–224.
[16] V. Berbenni, A. Marini, J. Anal. Appl. Pyrolysis 62 (2002) 45–62.

[17] P. Hartman, P. Bennema, J. Cryst. Growth 49 (1980) 145–156.
[18] M.-R. Huang, C.-W. Lin, H.-Y. Lu, Appl. Surf. Sci. 177 (2001) 103–113.
[19] J.M. Paulsen, C.L. Thomas, J.R. Dahn, J. Electrochem. Solid State Lett. 147 (2000) 861–868.
[20] S. Gopukumar, K.Y. Chung, K.B. Kim, Electrochim. Acta 49 (2004) 803–810.
[21] Q. Wu, X. Li, M. Yan, Z. Jiang, Electrochem. Commun. 5 (2003) 878–882.
[22] K.M. Shaju, G.V. Subbarao, B.V.R. Chowdari, J. Electrochem. Soc. 150 (2003) A1–A13.